machines

Article

Research on PID Controller of Excavator Electro-Hydraulic System Based on Improved Differential Evolution

Wei Ma [1,2], Shoulei Ma [1,2], Wenhua Qiao [1,2], Donghui Cao [3] and Chenbo Yin [1,2,*]

[1] United Institute of Excavator Key Technology, Nanjing Tech University, Nanjing 211816, China
[2] Institute of Automobile and Construction Machinery, Nanjing Tech University, Nanjing 211816, China
[3] SANY Group Co., Ltd., Suzhou 215300, China
* Correspondence: yinchenboiacm@163.com

Abstract: An electrical hydraulic control system (electro-hydraulic system) is thought to be a key component in excavator operation systems. Control methods with fixed parameters may not yield optimal system performances because a hydraulic system has various nonlinear uncertainties due to the leakage and compressibility of the fluid medium. Hence, a novel PID controller based on improved differential evolution (IDE) is introduced to excavator electro-hydraulic systems for interconnected hydraulic systems. The proposed algorithm not only adjusts the PID parameters of the different working conditions but also adjusts the scaling factor and crossover probability. Then, the proposed PID controller based on IDE and the excavator bucket control system are modeled and simulated on the MATLAB simulation platform. The simulation results demonstrate that the proposed controller has better performance in settling time, rise time, and convergence speed compared to the PID controller based on standard differential evolution and the Ziegler–Nichols (ZN) PID controller with a novel object function. Eventually, the IDE-PID controller is assessed on a 23-ton excavator, and good transient behavior and trajectory accuracy are obtained in comparison to the SDE-PID controller.

Keywords: excavator; PID controller; trajectory tracking; step response

Citation: Ma, W.; Ma, S.; Qiao, W.; Cao, D.; Yin, C. Research on PID Controller of Excavator Electro-Hydraulic System Based on Improved Differential Evolution. *Machines* **2023**, *11*, 143. https://doi.org/10.3390/machines11020143

Academic Editors: Qun Chao, Ruqi Ding and Min Cheng

Received: 23 November 2022
Revised: 12 January 2023
Accepted: 17 January 2023
Published: 20 January 2023

1. Introduction

In recent years, research on excavator control systems has been developed to greatly improve the efficiency and accuracy of working devices. Kim J et al. [1] designed a discrete time delay controller that combined time delay control (TDC) and terminal sliding mode control (TSMC) to decrease the influence of acceleration noise and achieve high position control tracking accuracy. Jianpeng S et al. [2] proposed a velocity and position combined control strategy based on mode switching; a strategy was found to decrease the operating velocity fluctuation and positioning error to the target position by approximately 1 mm. An online learning control method based on echo-state networks in [3] was employed to control a hydraulic servo system, which only used input and output signals, and the desired forces and trajectory were achieved in a simulation environment. Wang et al. [4] proposed a fuzzy logic control method that can improve energy distribution and fuel economy without sacrificing any of the system performance. In addition, sliding mode control [5], neural networks [6], and LS-SVM [7] have been tested for the control of hydraulic excavators.

Despite the wide utilization of many novel intelligent control algorithms in excavators, the simple structure, reliable performance, and robustness of the PID control make it irreplaceable. The change in the PID control parameters has a significant influence on control accuracy and efficiency. Therefore, the majorization of PID control parameters has gained extensive attention from researchers. To optimize the parameters, many algorithms, such as ant colony optimization (ACO) [8], particle swarm optimization (PSO) [9,10], and genetic algorithms (GAs) [11], have been applied. On the other hand, the "cross-coupled control" algorithm [12], which couples independent axis control and contour control with each other, has been demonstrated to reduce trajectory error.

The differential evolution (DE) algorithm is a global optimization algorithm that was proposed by Storn and Price [13] in 1997. It commonly consists of four steps: initialization, variation, crossover, and selection. Because it does not depend on the initial value and has fast convergence, few control parameters, and easy implementation, the differential evolution algorithm is widely used in the field of industrial control [14]. Moreover, DE can be applied not only in the field of continuous optimization but also in the field of discrete optimization. Therefore, it is also highly suitable for the field of digital control (DSP). These characteristics qualify DE for the control of the excavator.

This paper presents a parameters optimization approach for the PID controller by improved differential evolution (IDE). The PID controller will be discussed based on the valve-controlled asymmetrical cylinder model. The rest of paper will be organized as follows: the kinematics model of the excavator and control objective will be described in Section 2; Section 3 will show the detail of a mathematical model of the excavator electro-hydraulic system. The principles of the standard differential evolution (SDE) and the improved differential evolution (IDE) algorithms will be presented in Section 4. The optimization results of the PID parameters will be shown by a comparison of the simulation and experiments in Section 5. Finally, the conclusions of this paper will be drawn in Section 6.

2. System Structure

In this paper, the research focuses on the control problem of a SANY 23t electro-hydraulic excavator. The system consists of a three-subsystem pilot control subsystem, a main control subsystem, and an executive body subsystem. As shown in Figure 1, the pilot control subsystem includes joysticks, a pilot valve, and a pilot pump. Double pumps, a main valve, an engine, and a controller make up the main control subsystem. The executive body subsystem consists of a boom, an arm, bucket cylinders, and different kinds of sensors (displacement sensors, pressure sensors, speed sensors, and so on). According to the actual operation cycle, the electrical signal produced by the joysticks controls the pilot valve and produces pressure. Then, the pilot control pressure causes the corresponding displacement of the main valve spool, and the main control pressure makes the executive body generate force and displacement. The sensor feeds back the execution result to the controller. On the other hand, the engine and pumps provide power for the entire system.

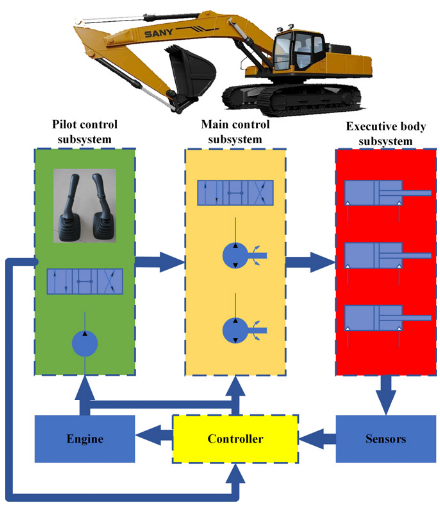

Figure 1. Overview of the SY235C8 hydraulic system.

2.1. *Kinematics of the Electronic-Hydraulic System for the 23t Excavator*

To estimate the position of the bucket tip, the kinematic model of the excavator working device is established. If the slewing of the excavator is not considered, the working device can be regarded as a 3 DOF manipulator.

Considering the kinematics analysis presented in Figure 2, the boom coordinate system is set up at the joint corner of point O_1, and θ_1 is the angle of the boom joint. O_2 is the hinge point of the arm and the boom; the arm coordinate system is set up there, and θ_2 is the angle of the arm joint. O_2 is the hinge point of the bucket and the arm; the bucket coordinate system is set up there, and θ_3 is the angle of the bucket joint. O_4 is the tip of the bucket.

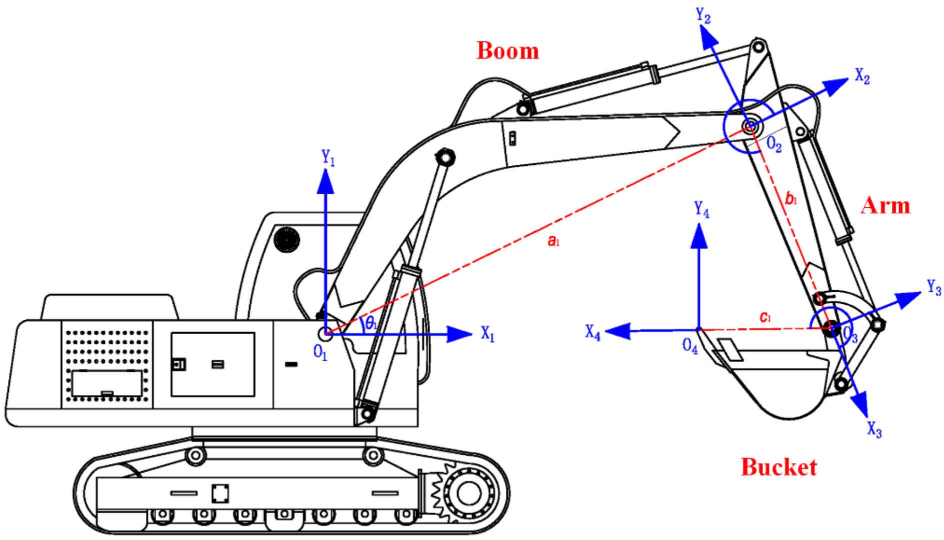

Figure 2. D-H coordinate system of excavator working device.

According to the established D-H coordinate system and the vector algorithm, the vector $\overrightarrow{O_1O_2}$,$\overrightarrow{O_2O_3}$ and $\overrightarrow{O_3O_4}$ can be expressed by Equation (1):

$$\begin{cases} \overrightarrow{O_1O_2} = (a_1\cos\theta_1, a_1\sin\theta_1, 0) \\ \overrightarrow{O_2O_3} = (a_2\cos(\theta_1+\theta_2), a_2\sin(\theta_1+\theta_2), 0) \\ \overrightarrow{O_3O_4} = (a_3\cos(\theta_1+\theta_2+\theta_3), a_3\sin(\theta_1+\theta_2+\theta_3), 0) \end{cases} \tag{1}$$

Assuming that the coordinates of the bucket tip O_4 are (x, y, z), then t O_4 can be calculated by Equation (2):

$$\begin{cases} x = a_1\cos\theta_1 + a_2\cos(\theta_1+\theta_2) + a_3\cos(\theta_1+\theta_2+\theta_3) \\ y = a_1\sin\theta_1 + a_2\sin(\theta_1+\theta_2) + a_3\sin(\theta_1+\theta_2+\theta_3) \\ z = 0 \end{cases} \tag{2}$$

As is given in Equation (2), the position coordinates of the tip of the excavator bucket are determined by the parameters θ_1,θ_2,θ_3 and a_1,a_2,a_3. For a certain excavator, a_1,a_2,a_3 are the known fixed parameters. Therefore, as long as the values of θ_1,θ_2,θ_3 and these three parameters are precisely measured, the forward kinematic solution of the working device can be completed.

2.2. System Control Objective

The control objective of this paper is to develop control rules and to minimize the trajectory tracking errors. The objective formulation can be given as:

$$\lim_{t\to\infty}\left[e_x\ e_y\ e_z\right]^T = [0\ 0\ 0]^T \left[e_x\ e_y\ e_z\right]^T = \left[\left|O_{4actual} - O_{4ref}\right|\right]^T \tag{3}$$

where $O_{4actual}$ and O_{4ref} are the actual and the reference positions of the bucket tip; e_x,e_y, and e_z are the errors in the x, y, and z axis directions, respectively.

3. Control System Design

3.1. PID Control System Description

Standard PID control law consists of three parameters: proportion, integration, and differentiation. They compare the collected data with the reference data and compute the new input values based on the error of comparison. It could be calculated as:

$$\begin{cases} e(t) = y(t) - r(t) \\ u(t) = K_p e(t) + K_I \int_0^t e(t)dt + K_D \frac{de(t)}{dt} \end{cases} \quad (4)$$

where the difference between the actual position $y(t)$ and the reference position $r(t)$ can be given by $e(t)$; the input signal of the system can be represented by $u(t)$; K_p, K_I, and K_D are the proportional gain, integral gain, and derivative gain parameters, respectively.

3.2. Electro-Proportional System Formulation

Four different cylinders drive, respectively, the boom, the arm, and the bucket, and they are driven by three electro-hydraulic proportional systems. The theories in the three systems are the same except for some of the size or geometry parameter values. Figure 3 presents the signal processing routine in the electro-hydraulic proportional system. The first stage is the proportional gain stage, the second stage is the electro-hydraulic stage, and the valve-controlled asymmetrical cylinder and feedback, respectively, are the third and fourth stages.

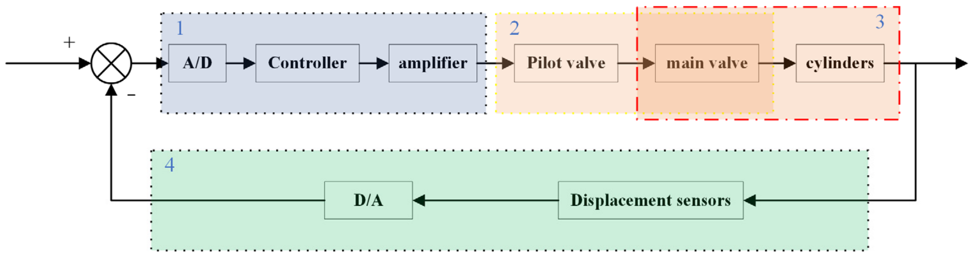

Figure 3. The principle diagram of electro-hydraulic proportional system.

3.2.1. Proportional Gain Stage

As shown in Figure 4, the signal transmission process is divided into four parts and they are the electric control, pilot circuit, main circuit, and feedback part. The pilot valve works based on a proportional electromagnet; the input signal of it is the current, and the signal output from the joystick is a voltage signal; so, the first stage can be considered as a proportional gain stage, which can be given as:

$$K_a = \frac{i}{u} \quad (5)$$

where i is the output current signal required by the pilot valve; u is the input voltage signal produced by the joystick; and K_a is the amplification coefficient of the proportional gain stage.

3.2.2. Electro-Hydraulic Proportional Stage

The electro-hydraulic proportional stage builds the link between the electrical signal and the physical signal. The ratio electromagnet is converted into force according to the magnitude of the current passing through the energized coil and acts on the spool of the pilot valve. Owing to the values having little influence on the total system, the dynamic of the pilot valve is ignored, and this stage can simplify into a linear model:

$$\frac{K_b}{Ts+1} = \frac{x_v}{i} \quad (6)$$

where i is the input current signal; x_v denotes the displacement of the main valve spool generated by pilot pressure; K_b is the amplification coefficient; T is the time constant; and the parameter s represents the operator in the Laplace transform, which has no specific meaning.

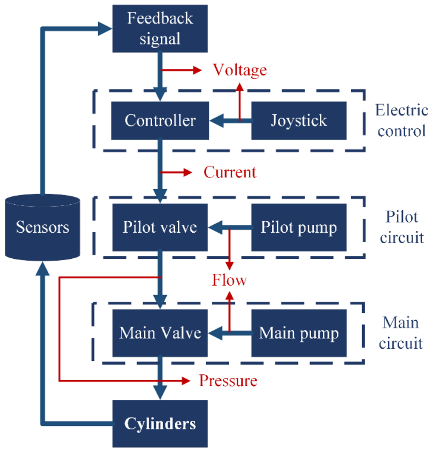

Figure 4. The signal transmission diagram of electro-hydraulic system.

3.2.3. Valve-Controlled Cylinder Stage

Figure 5 shows the principle of the valve-controlled asymmetrical cylinder system. Some assumptions are made before the mathematical model's establishment of this stage. Firstly, the flow at the throttle window is turbulent, and the effect of liquid compression can be ignored in the valve. Secondly, there is no delay in the response of the valve; that is, the flow rate change can occur instantly in response to the change in the spool displacement and the valve pressure drop. Thirdly, the supply pressure of the hydraulic oil remains unchanged, and the pressure of the oil return channel is zero. Finally, the leakage of the valve is ignored, and the internal and external leakage of the hydraulic cylinder are idealized as laminar flow.

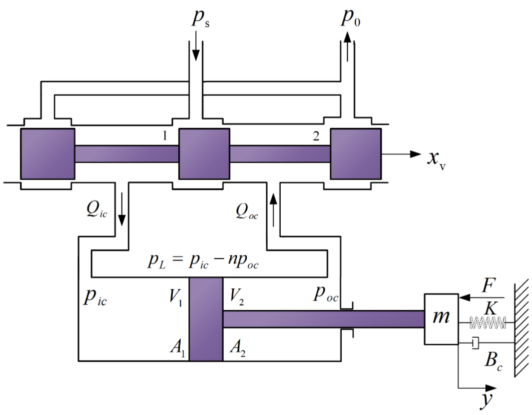

Figure 5. Valve-controlled asymmetrical cylinder system.

Under this assumption condition, the load flow equation of the pilot system after linearization can be written as:

$$Q_{pL} = K_q x_v - K_p P_L \tag{7}$$

where K_q and K_p are the flow gain coefficient and flow pressure coefficient, respectively; Q_{pL} denotes the load flow of the pilot valve; P_L represents the load pressure, and it can be obtained by:

$$P_L = p_{ic} - np_{oc} \tag{8}$$

where p_1 and p_2 are the pressures of the rod and the rodless chambers in the cylinder, respectively. n ($n = \frac{A_2}{A_1}$, A_1 is the effective working area of rod chamber, and A_2 is the effective working area of the rodless chamber) is the flow ratio between the rod and the rodless chambers flowing into and out of the asymmetrical hydraulic cylinder.

According to the principle of thin-walled orifice throttling, the flow rates through orifices 1 and 2 can be written as:

$$\begin{aligned} Q_{ic} &= C_d \omega x_v \sqrt{\tfrac{2}{\rho}(p_s - p_{ic})} \\ Q_{oc} &= C_d \omega x_v \sqrt{\tfrac{2}{\rho}(p_{oc} - 0)} \end{aligned} \tag{9}$$

where Q_{ic} and Q_{oc} denote the inside and the outside flow of the rod and the rodless chambers; C_d is regarded as the flow coefficient of the orifice; ω is the area gradient of the orifice; ρ represents the oil density; and p_s is the supply oil pressure. Therefore, the flow ratio of the rod and the rodless chambers can be expressed as:

$$n = \frac{Q_{oc}}{Q_{ic}} = \sqrt{\frac{p_{oc}}{p_s - p_{ic}}} \tag{10}$$

The continuity flow equations of the rod and the rodless chambers of the valve-controlled asymmetrical cylinder can be derived as:

$$\begin{aligned} Q_1 &= C_{iL}(p_{ic} - p_{oc}) + C_{oL}p_{ic} + \tfrac{V_1}{\beta_e}\tfrac{dp_{ic}}{dt} + \tfrac{dV_1}{dt} \\ Q_2 &= C_{iL}(p_{ic} - p_{oc}) + C_{oL}p_{oc} + \tfrac{V_2}{\beta_e}\tfrac{dp_{oc}}{dt} - \tfrac{dV_2}{dt} \end{aligned} \tag{11}$$

where C_{iL} and C_{oL} denote the inside and outside leakage coefficient of the main valve; V_1 and V_2 represent the volumes of the rod and the rodless chambers; and β_e denotes the effective bulk elastic modulus.

Combining Equations (8) and (10), the pressure of the rod and the rodless chambers can be expressed as:

$$\begin{aligned} p_{ic} &= \tfrac{n^3 p_s + p_L}{1+n^3} \\ p_{oc} &= \tfrac{n^2(p_s - p_L)}{1+n^3} \end{aligned} \tag{12}$$

Combining Equations (7)–(12), the continuity equation of the hydraulic cylinder chambers can be calculated as:

$$Q_{pL} = A_1\frac{dy}{dt} + \frac{V}{2(1+n^2)\beta_e}\frac{dp_L}{dt} + \frac{1+n}{1+n^2}C_{iL}p_L + \frac{1}{1+n^2}C_{oL}p_l \tag{13}$$

The y and V in Equation (13) are the displacement of the rod and the total volume of the cylinder chamber, respectively.

Assuming that the friction, leakage, and compression of the hydraulic oil are ignored, then the force balance equation of the t valve-controlled asymmetrical cylinder system will be derived as:

$$m\frac{d^2y}{dt^2} = A_1 p_L - B_c\frac{dy}{dt} - Ky - F \tag{14}$$

where the total mass of the piston, hydraulic oil, and load acting on the piston can be calculated by parameter m; B_c represents the viscous damping coefficient of the piston and load; K denotes the spring rate of the load; and F is the external load acting on the piston.

Due to the actual working process of the excavator, the elastic stiffness of the load is much smaller than the other parameters of the system; so, it is usually ignored.

Equations (7), (13), and (14) can describe the properties of the valve-controlled asymmetric cylinder system. When the elastic stiffness of the external load is not considered, the fusion of the three Equations (7), (13), and (14) can eliminate the intermediate parameters, and after simplification and Laplace transform, the transfer function of the displacement of the piston rod and the displacement of the pilot valve spool and the load force can be obtained.

$$y = \frac{\frac{K_q}{A_1} x_v - \frac{K_{total}}{A_1{}^2}\left(\frac{V}{2(1+n^2)\beta_e K_{total}} s + 1\right) F}{\left(\frac{s^2}{\omega_h{}^2} + \frac{2\xi_h}{\omega_h} s + 1\right) s} \tag{15}$$

where K_{total} denotes the total flow gain coefficient; ξ_h represents the comprehensive damping coefficient of the system; ω_h is the hydraulic resonance frequency; and s is the Laplace operator. They can be expressed as:

$$K_{total} = \frac{1+n}{1+n^2} C_{iL} + \frac{1}{1+n^2} C_{oL} + K_p \tag{16}$$

$$\xi_h = \frac{K_{total}}{A_1} \sqrt{\frac{(1+n^2)\beta_e m}{2V}} + \frac{B_c}{2A_1} \sqrt{\frac{V}{2(1+n^2)\beta_e m}} \tag{17}$$

$$\omega_h = \sqrt{\frac{2(1+n^2)\beta_e A_1{}^2}{Vm}} \tag{18}$$

3.2.4. Feedback Stage

The feedback stage is a normal proportional stage based on displacement sensors. Its mathematical model can be given as:

$$K_{fb} = \frac{u_s}{y} \tag{19}$$

where K_{fb} is the proportional coefficient; u_s denotes the output voltage of displacement sensor; and y represents the displacement of the hydraulic cylinder. The block diagram of the valve-controlled cylinder system is shown in Figure 6, according to the above derivation of formulas.

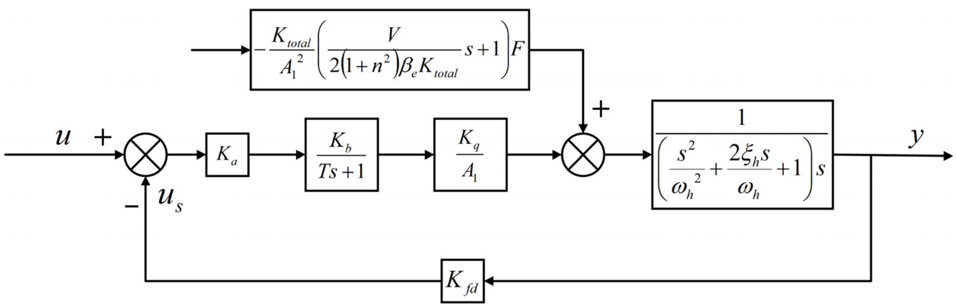

Figure 6. Block diagram of the valve-controlled cylinder.

4. SDE and IDE Algorithm

The differential evolution (DE) algorithm has been widely utilized in the field of control parameter optimization since its introduction in 1997 by Storn, R. The controller parameter tuning based on the DE algorithm and its application to the load frequency control (LFC) of a multi-source power system has been presented in paper [15]. Miguel G. et al. proposed a DE algorithm based on a control adaptation, and it has proved to have a better control effect on a direct current motor. Paper [16] applied the DE algorithm to settle a vehicle routing problem with backhauls for a catering firm. On the other hand, the researchers have also conducted lots of work on the improvements of the DE algorithm. The DE variants have been utilized in lots of fields, such as mathematics, computer science, operations research, engineering, economics physics, and biology due to their excellent performance [17]. This paper will apply the standard differential evolution (SDE) and the improved differential evolution (IDE) algorithms in the tuning of the PID control parameters. The detail and comparison of the algorithms will be shown in this section.

4.1. SDE

The differential evolution algorithm is a super-heuristic group intelligence optimization method based on evolutionary ideas and population differences. Its core idea is to solve global optimization problems through cooperation and competition among individuals within the population. As with most evolutionary algorithms, differential evolution algorithms are also divided into initialization, mutation, crossover, and selection.

Initialization: During initialization, a random original population is generated within the value range of the solution. The initialization of DE can be given as:

$$\left\{ X_i(0) \middle| x_{i,j}^L \leq x_{i,j}(0) \leq x_{i,j}^U; i = 1,2,\cdots,NP; j = 1,2,\cdots,D \right\} \tag{20}$$

where $X_i(0)$ denotes any individual; $x_{i,j}^L$ and $x_{i,j}^U$ represent the upper and lower limits of the search interval, respectively; NP is the size of population; and D denotes the dimension of problem.

Mutation: During mutation, the mutation vector v_i^g will be generated for each target vector x_i^g at any generation g as:

$$v_i^g = x_{r1}^g + F\left(x_{r2}^g - x_{r3}^g\right) \tag{21}$$

where F denotes the scaling factor, and $r1, r2, r3 \in \{1, 2, \cdots, NP\}$ are randomly selected from the population and are different from each other. According to Storn's suggestion, the initial value of F is 0.5, and the values vary from 0.5 to 1.

Crossover: After mutation (Figure 7), an intermediate vector u_i^g, called the test vector, will be generated from target vector x_i^g and the mutation vector v_i^g using a crossover coefficient CR as:

$$u_{i,j}^g = \begin{cases} v_{i,j}^g & if\ rand_j \leq CR & CR \in (0,1) \\ x_{i,j}^g & otherwise & j = 1,2,3\ldots D \end{cases} \tag{22}$$

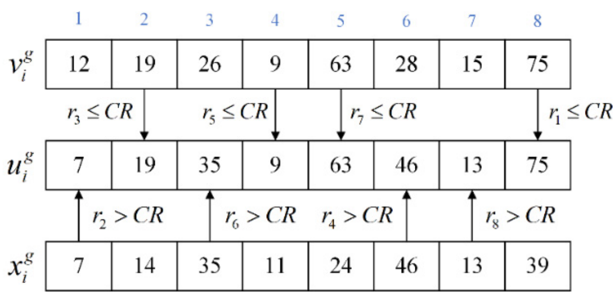

Figure 7. The process of crossover operation.

Selection: When the mutation and crossover are finished, the next generation will be produced based on the fitness functions ($f\left(u_i^g\right)$ and $f\left(x_i^g\right)$) of the target vector and test vector. This operation can be expressed as:

$$x_i^{g+1} = \begin{cases} u_i^g & if\ f\left(u_i^g\right) \leq f\left(x_i^g\right) \\ x_i^g & otherwise \end{cases} \tag{23}$$

From Equations (20)–(23), the flowchart of the SDE is shown in Figure 8.

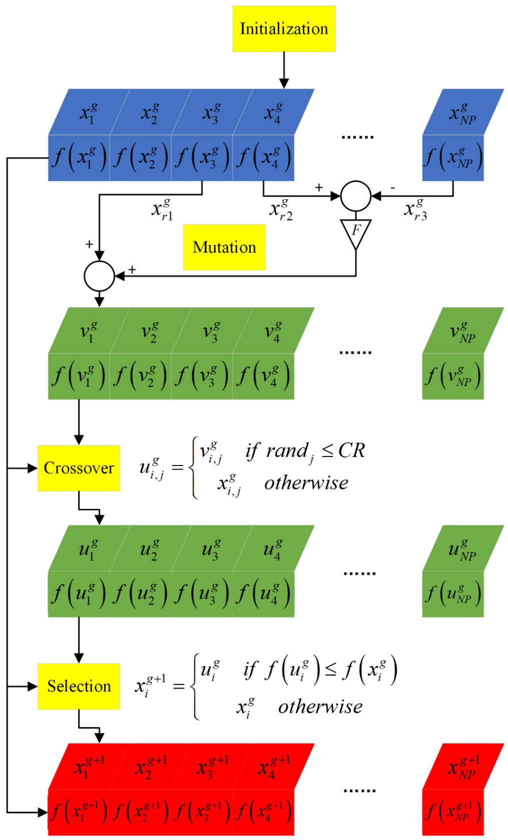

Figure 8. The flowchart of SDE.

According to the above derivation, the standard differential evolution algorithm has fewer operation parameters than the other evolutionary algorithms. These algorithm parameters are mainly population size NP, problem dimension D, scaling factor F, and crossover probability CR. The performance of the algorithm largely depends on the values of these parameters, and papers [18–22] have conducted research on the selection of the parameters.

4.2. IDE

As a group optimization algorithm, DE has the characteristics of fewer control variables, low space complexity, and easy implementation. However, DE also inevitably has some problems, such as search stagnation and premature convergence. To solve these problems, some improvements have been performed as follows.

(1) Scaling factor F self-adaptation

The decision regarding the DE algorithm parameters has an important impact on the performance of the algorithm. In the DE algorithm, the scaling factor F is to scale the difference vector corresponding to everyone in the population, to determine the search range of the current individual, and to generate a mutation vector. In practical applications when F is unchanged, if F is too large, the speed of the algorithm convergence will be slow, and the obtainable probability of the global optimal solution will be reduced. If F is too small, it will lead to a decrease in the diversity of the population and be premature. So, the value of parameter F will change based on the number of iterations. At the beginning of the iteration, F is larger, which can maintain the diversity of the population. The value of parameter F will decrease as the number of iterations increases; this can save excellent population information in order to avoid a local optimal solution. The self-adaptation factor λ is given as follows.

$$\lambda = e^{1-\frac{Gm}{1+Gm-G}} \tag{24}$$

where G_m denotes maximum number of iterations, and G is the current number of iterations. So, the scaling factor F will given as follows.

$$F = F_0 2^{\lambda} \tag{25}$$

where F_0 is the initial coefficient of variation, and $F_0 = 0.9$ in this thesis. During the mutation of each generation, the value of F will decrease continuously as the number of iterations increases.

(2) Crossover probability CR self-adaption

Parameter CR has an impact on the diversity of the population and determines which individual could be transformed. On one hand, the small value of CR will make the number of individuals transformed in the population lower; the characteristics of the solution in the current population are more reserved, which maintains the stable progress of the evolution process. On the other hand, if CR is large, the greater transformation in the population will increase the population diversity, and this can avoid local optimal solutions. The self-adaptive crossover coefficient CR can be given as follows.

$$CR_i = \begin{cases} CR_i + (CR_u - CR_l)\frac{f_i - f_{best}}{f_{max}} & f_i \geq f_{best} \\ CR_i & f_i < f_{best} \end{cases} \tag{26}$$

where CR_u and CR_l denote the upper and lower limits of the value CR, respectively. f_{best} and f_{max} are the best and maximum individual objective function values of the current population. f_i and CR_i are the objective function value and the cross coefficient of the i-th generation individual. The CR will change as the population evolves and the individual objective function value changes, which ensures the stability of the algorithm convergence.

4.3. Comparison of SDE and IDE

4.3.1. Objective Function and Fitness Value

As mentioned above, the DE algorithm can obtain the optimal solution of a control problem, and the objective function is the mathematical description that defines the performance of the control system. In general, the objective function can be defined according to our desired performance specifications for a controller design. Integrated squared error (ISE), integrated absolute error (IAE), and the target of the integral of time multiplied absolute error (ITAE) are usually considered as the criteria for control system performance [23]. This paper adopts the absolute error and increases the square term of the control input as the optimization objective function of the differential evolution algorithm to improve the stability of the system. Therefore, the objective function J can be expressed as:

$$J = \int_0^{\infty} (\omega_1 |e(t)| + \omega_2 u^2(t))dt + \omega_3 t_r \tag{27}$$

where ω_1, ω_2, and ω_3 denote the weights of each indicator, and t_r represents the settling time of the control system; $e(t)$ is the systematic error, and $u(t)$ is the system output. However, the objective function is inversely proportional to the performance of the control system. The larger the objective function is, the worse the control performance will be. In order to be proportional to the performance of the control system, the fitness value f of the individual can be written as the inverse of the objective function J ($f = \frac{1}{J}$).

4.3.2. The Steps for Optimization of PID Parameters

The PID parameters will be tuned automatically by the improved DE; the steps are summarized as follows:

Step 1. Randomly generate original population x^g, which is composed of NP individuals.
Step 2. Scaling factor F and fitness value f of everyone will be calculated according to Equations (24), (25), and (27).

Step 3. Calculate and generate mutation vector v^{g0} and fitness of everyone according to Equation (21).
Step 4. Calculate and generate crossover probability CR and test vector u^{g0} by Equations (26) and (22). Update the fitness value f of everyone.
Step 5. Generate new population x^{g0+1} and update the fitness value f to execute the next iteration.
Step 6. Repeat steps (3)–(5) until the iteration number is to the limits and stop the algorithm.

4.3.3. Simulation Results

The performance of the proposed IDE was tested by applying it to an excavator electro-hydraulic system, and the details of the simulation results are shown below. The controller system and the optimization process were designed in MATLAB software, and the hydraulic system was designed in AMESim [24] (Figure 9). The co-simulation of MATLAB and AMESim has been widely accepted by many works for testing characteristics such as the dead band of a main valve and the asymmetric dynamic characteristics of a valve-controlled asymmetric cylinder. Some examples are the research on high tracking control [10,25], the efficiency of hydraulic systems [26,27], and energy regeneration systems [28,29].

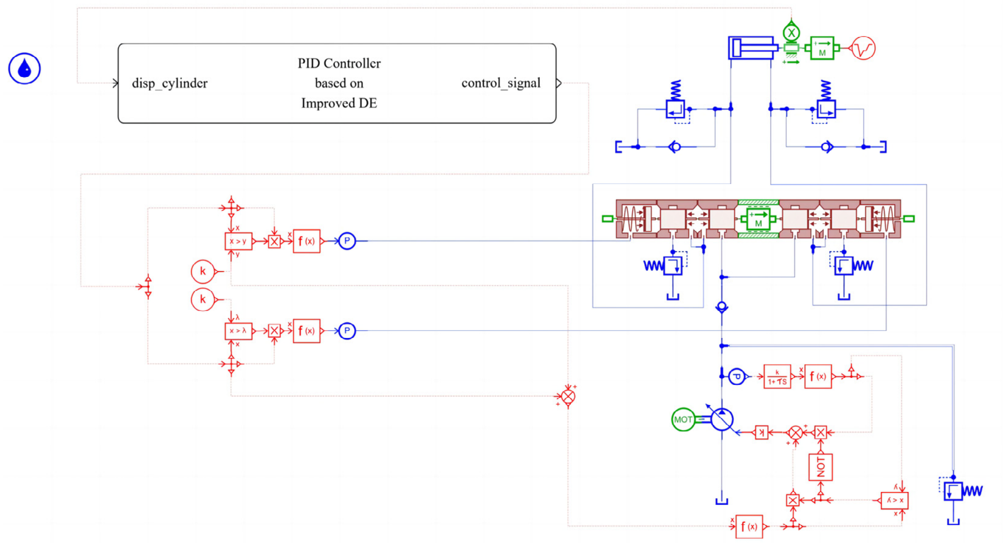

Figure 9. Co-simulation model of bucket system.

Then, the performance of different tuning techniques was evaluated by the fitness function f with the transient response characteristics of the control system, i.e., the overshoot and settling time.

The research on the selection of the parameters of the SDE algorithm started very early, but we did not find an excellent theory to determine them. So far, the ranges of parameters were decided by prior knowledge. So, we adopted the strategy of the selection of parameters conducted by Ronkkonen et al. [30] and Suganthan P N et al. [31]. The other parameters mentioned in the simulation are listed in Table 1. As mentioned in most papers, we use the step signal as the test signal of the excavating electro-hydraulic system due to its easy usability and implementation in software. The step responses of a 23-ton excavator bucket electro-hydraulic system with a reference $yd = 1$ m will be compared. On the other hand, the convergence curve of the SDE-PID controller is compared with the convergence curve of the IDE-PID controller. The simulation results of three different controllers are shown in Table 2.

Table 1. Parameters of SDE and IDE tuning based on PID controller.

Symbol	Parameters	SDE	IDE
NP	Number of individuals	50	50
F	Mutation scaling factor	0.9	unfixed
CR	Crossover probability	0.8	unfixed
D	Dimension of issue	3	3
G	Maximum number of iterations	100	100
ω_1	Weight 1	0.999	0.999
ω_2	Weight 2	0.001	0.001
ω_3	Weight 3	2	2
$[L_1, U_1]$	Search range of K_p	[0, 20]	[0, 20]
$[L_2, U_2]$	Search range of K_i	[0, 10]	[0, 10]
$[L_3, U_3]$	Search range of K_d	[0, 10]	[0, 10]

Table 2. Comparisons of controller tuning methods with step reference.

Tuning Method	Rise Time (s)	Settling Time (s)	Number of Iterations	Best J
ZN	1.55	3.27	/	/
SDE	1.17	2.37	81	2.35
IDE	**0.93**	**1.84**	**57**	**1.74**

The controller tuning method ZN obtained the highest rise time and settling time, which were 1.55 s and 3.27 s, respectively. Compared with the ZN tuning method, the proposed SDE and IDE tuning methods obtained better performances on rise time (1.17 s and 0.93 s) and settling time (2.37 s and 1.84 s). As shown in Table 2, the tuning method IDE not only obtains a shorter time for the steady state of the excavator bucket control system but also achieves a smaller number of iterations (57 vs. 81) and a smaller best J (1.74 vs. 2.35).

Figure 10a,b demonstrate the step responses of the excavator bucket electro-hydraulic system and convergence curves of objective function J. On the other hand, the sinusoidal wave is used to track the errors of the electro-hydraulic system. The sinusoidal responses and tracking errors are demonstrated in Figure 11. It can be easily seen in the figure that a lag time of 0.05 s exists between the reference signal (a sinusoidal wave whose frequency is 1 Hz and amplitude is 1 m) and the output signal for the IDE-PID controller. Compared with the other two controllers, the lag time of the IDE-PID controller is the shortest.

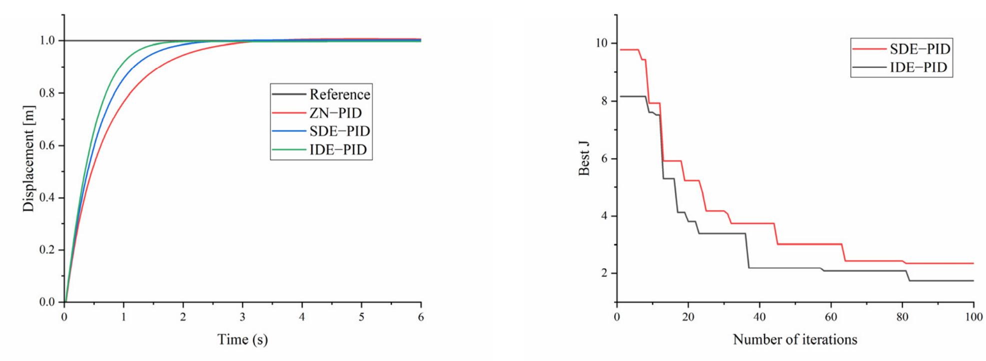

(**a**) (**b**)

Figure 10. (**a**) Comparisons of step responses and (**b**) convergence curves of SDE-PID and IDE-PID.

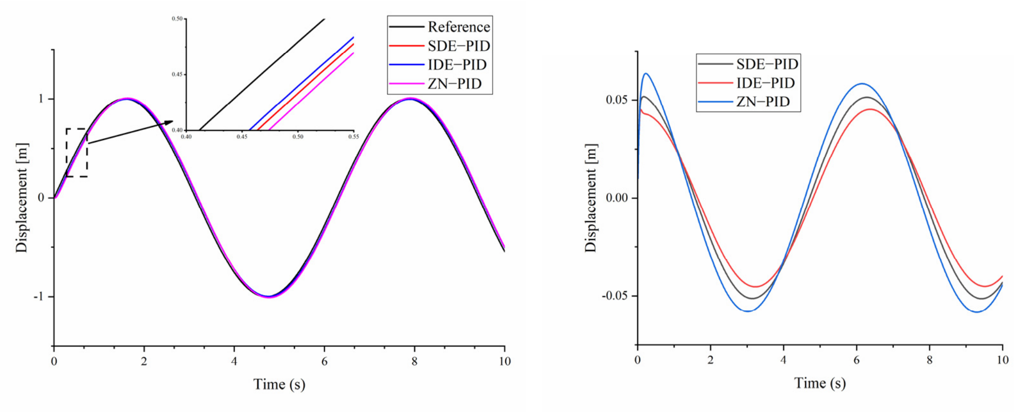

(**a**) (**b**)

Figure 11. (**a**) Comparisons of sinusoidal responses and (**b**) tracking errors.

According to the above discussion, the proposed IDE always has a better advantage, with a new objective function J, in iterations and convergence speed than the SDE under the parameters presented in Table 1. It can be concluded that the co-simulation shows that the proposed SDE-PID controller obtained better performances in settling time, rise time, and lag time.

5. Experiments

5.1. Experiment Platform

To verify the effectiveness of the proposed control method, some trajectory control must be implemented on the excavator. Some sensors were installed on the excavator to measure the displacement of the cylinder and the pressure of the electro-hydraulic system, as shown in Figure 12.

The displacement sensor is placed outside the hydraulic cylinder, and the pressure sensor is placed inside the oil circuit. The analog signals produced by the sensors will be transferred into digital signals with a DAQ and DSP and communicated with the designed controller via USB-CAN. Table 3 shows the main parameters of the sensors.

Table 3. Sensors and their parameters used in the experiments.

Sensors	Type	Main Parameters
DSP controller	283H	32-bit, duty cycle < 1 ms
DAQ card	NI USB 6215	16-bit, 8AI/2AO, 4DI/4DO
Displacement sensor	WDS-2500	Scale 0–2500 mm, 0.2 accuracy class
Pressure sensor	625 T4-16-Z23	Scale 0–400 bar, 0.2% FS accuracy
USB-CAN	USBCAN-II PRO	32-bit CPU

5.2. Experiments Results

Experimental conditions: When the trajectory tracking experiments were implemented, the excavator was not rotated. The leveling operation was selected to experiment with the motion because of the frequency executed in the working loop. Therefore, the excavator performed the leveling operation from the starting point (4800,0,0) to the end point (6600,0,0) under no load conditions.

Figure 12. Laboratory 23-ton excavator trajectory control experiment platform: (**a**) 23-ton excavator, (**b**) 283H DSP controller, (**c**) displacement sensor of bucket, (**d**) displacement sensor of bucket, (**e**) displacement sensor of bucket, (**f**) NI 6215 DAQ card, (**g**) data collection system.

According to the relationship between the extension and the retraction of the cylinder and the coordinates obtained by Equation (2), the cylinder displacement obtained by the three controllers (ZN-PID, SDE-PID, and IDE-PID) is converted into the bucket tip coordinates through the kinematic calculation. Figure 13 shows their tracking results. The maximum error between the desired and the actual trajectories is 107.1 mm by ZN-PID. However, the maximum error is reduced to 74.3 mm and 49.5 mm by SDE-PID and IDE-PID, respectively. Therefore, it is obvious that SDE-PID and IDE-PID have better control performances than ZN-PID. Moreover, the proposed IDE-PID has a smaller maximum error and improves the trajectory tracking accuracy by 33.4%.

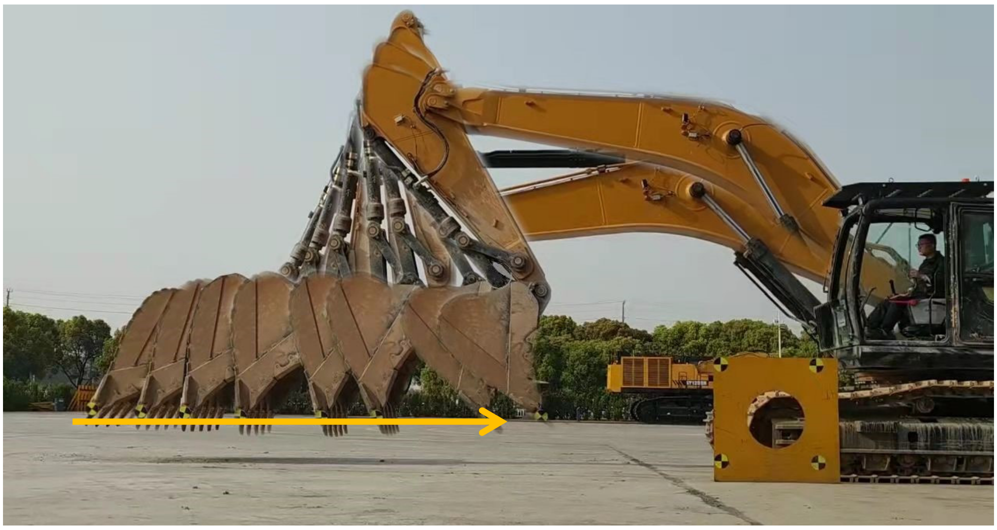

(**a**)

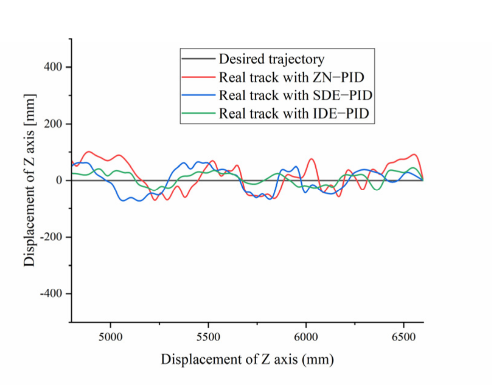

(**b**)

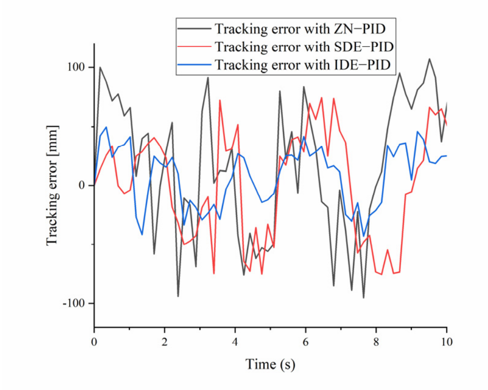

(**c**)

Figure 13. (**a**) Schematic diagram of experimental results (the arrow indicated the leveling operation), (**b**) trajectory tracking results of bucket tip, and (**c**) tracking errors when excavator performs leveling operation.

6. Conclusions

A novel IDE algorithm was proposed and used in the parameter tuning of the PID controller for excavators. Compared with the SDE algorithm, the proposed algorithm has made adaptive improvements to the scale factor F and the crossover probability CR, which overcomes the shortcomings of the traditional algorithm of slow convergence velocity and easy local convergence. Then, the PID controller based on IDE tuning was designed.

The step signal and sinusoidal wave were used as references for the comparison of the performances of IDE-PID and the other two controllers (SDE-PID and ZN-PID). The simulation results show that the proposed novel IDE-PID controller has better performance on the settling time, rise time, and convergence velocity with the new objective function J.

Finally, the experiments implemented on a 23-ton excavator demonstrated that the tracking error was reduced by using the IDE-PID controller compared with the other controllers. Due to the nonlinearity of the system and the variety of loads, the tracking error is still very large. Research on the influence of the load on the control algorithm will be further carried out in the future.

Author Contributions: Conceptualization, W.M.; Methodology, W.M.; Software, S.M.; Data curation, W.Q.; Project administration, D.C.; Funding acquisition, C.Y. All authors have read and agreed to the published version of the manuscript.

Funding: This work was supported by the National Key R&D Program of China (No. 2021YFB2011904).

Data Availability Statement: Not applicable.

Conflicts of Interest: The authors declare no conflict of interest.

References

1. Kim, J.; Jin, M.; Choi, W.; Lee, J. Discrete time delay control for hydraulic excavator motion control with terminal sliding mode control. *Mechatronics* **2019**, *60*, 15–25. [CrossRef]
2. Shi, J.; Quan, L.; Zhang, X.; Xiong, X. Electro-hydraulic velocity and position control based on independent metering valve control in mobile construction equipment. *Autom. Constr.* **2018**, *94*, 73–84. [CrossRef]
3. Park, J.; Cho, D.; Kim, S.; Kim, Y.B.; Kim, P.Y.; Kim, H.J. Utilizing online learning based on echo-state networks for the control of a hydraulic excavator. *Mechatronics* **2014**, *24*, 986–1000. [CrossRef]
4. Wang, D.; Lin, X.; Zhang, Y. Fuzzy logic control for a parallel hybrid hydraulic excavator using genetic algorithm. *Autom. Constr.* **2011**, *20*, 581–587. [CrossRef]
5. Won, D.; Kim, W.; Tomizuka, M. High Gain Observer Based Integral Sliding Mode Control for Position Tracking of Electro-hydraulic Servo Systems. *IEEE/ASME Trans. Mechatron.* **2017**, *22*, 2695–2704. [CrossRef]
6. Le Hanh, D.; Ahn, K.K.; Kha, N.B.; Jo, W.K. Trajectory control of electro-hydraulic excavator using fuzzy self tuning algorithm with neural network. *J. Mech. Sci. Technol.* **2009**, *23*, 149–160. [CrossRef]
7. Khalil, H.M.; El-Bardini, M. Implementation of speed controller for rotary hydraulic motor based on LS-SVM. *Expert Syst. Appl.* **2011**, *38*, 14249–14256. [CrossRef]
8. Duan, H.; Liu, S.; Wang, D.; Yu, X. Design and realization of hybrid ACO-based PID and LuGre friction compensation controller for three degree-of-freedom high precision flight simulator. *Simul. Model. Pract. Theory* **2009**, *17*, 1160–1169. [CrossRef]
9. Ye, Y.; Yin, C.B.; Gong, Y.; Zhou, J.J. Position control of nonlinear hydraulic system using an improved PSO based PID controller. *Mech. Syst. Signal Process.* **2017**, *83*, 241–259. [CrossRef]
10. Song, H.; Li, G.; Li, Z.; Xiong, X. Trajectory Control Strategy and System Modeling of Load-Sensitive Hydraulic Excavator. *Machines* **2023**, *11*, 10. [CrossRef]
11. Feng, H.; Yin, C.B.; Weng, W.W.; Ma, W.; Zhou, J.J.; Jia, W.H.; Zhang, Z.L. Robotic excavator trajectory control using an improved GA based PID controller. *Mech. Syst. Signal Process.* **2018**, *105*, 153–168. [CrossRef]
12. Lee, C.S.; Bae, J.; Hong, D. Contour control for leveling work with robotic excavator. *Int. J. Precis. Eng. Manuf.* **2013**, *14*, 2055–2060. [CrossRef]
13. Storn, R.; Price, K. Differential Evolution—A Simple and Efficient Heuristic for global Optimization over Continuous Spaces. *J. Glob. Optim.* **1997**, *11*, 341–359. [CrossRef]
14. Storn, R.; Price, K. *Differential Evolution: A Simple and Efficient Adaptive Scheme for Global Optimization over Continuous Spaces*; Technical Report TR-95-012; International Computer Science Institute: Berkeley, CA, USA, 2005.
15. Mohanty, B.; Panda, S.; Hota, P.K. Controller parameters tuning of differential evolution algorithm and its application to load frequency control of multi-source power system. *Int. J. Electr. Power Energy Syst.* **2014**, *54*, 77–85. [CrossRef]
16. Küçükoğlu, İ.; Öztürk, N. A differential evolution approach for the vehicle routing problem with backhauls and time windows. *J. Adv. Transp.* **2014**, *48*, 942–956. [CrossRef]
17. Pant, M.; Zaheer, H.; Garcia-Hernandez, L.; Abraham, A. Differential evolution: A review of more than two decades of research. *Eng. Appl. Artif. Intell.* **2020**, *90*, 103479.
18. Zhao, Z.; Yang, J.; Hu, Z.; Che, H. A differential evolution algorithm with self-adaptive strategy and control parameters based on symmetric Latin hypercube design for unconstrained optimization problems. *Eur. J. Oper. Res.* **2016**, *250*, 30–45.
19. Ghosh, A.; Das, S.; Chowdhury, A.; Giri, R. An improved differential evolution algorithm with fitness-based adaptation of the control parameters. *Inf. Sci.* **2011**, *181*, 3749–3765.
20. Wang, H.; Rahnamayan, S.; Sun, H.; Omran, M.G. Gaussian Bare-Bones Differential Evolution. *IEEE Trans. Cybern.* **2013**, *43*, 634–647. [CrossRef]
21. Meng, Z.; Pan, J.S.; Kong, L. Parameters with Adaptive Learning Mechanism (PALM) for the enhancement of Differential Evolution. *Knowl. Based Syst.* **2018**, *141*, 92–112. [CrossRef]
22. Zamuda, A.; Brest, J. Self-adaptive control parameters? randomization frequency and propagations in differential evolution. *Swarm Evol. Comput.* **2015**, *25*, 72–99. [CrossRef]
23. Hou, Y.-Y. Design and implementation of EP-based PID controller for chaos synchronization of Rikitake circuit systems. *ISA Trans.* **2017**, *70*, 260–268. [CrossRef] [PubMed]
24. Vasiliu, N.; Vasiliu, D.; Călinoiu, C.; Puhalschi, R. *Simulation of Fluid Power Systems with Simcenter Amesim*; CRC Press: Boca Raton, FL, USA, 2018.
25. Nguyen, T.H.; Do, T.C.; Nguyen, V.H.; Ahn, K.K. High Tracking Control for a New Independent Metering Valve System Using Velocity-Load Feedforward and Position Feedback Methods. *Appl. Sci.* **2022**, *12*, 9827. [CrossRef]
26. Heybroek, K.; Sahlman, M. A hydraulic hybrid excavator based on multi-chamber cylinders and secondary control—Design and experimental validation. *Int. J. Fluid Power* **2018**, *19*, 91–105. [CrossRef]

27. Qu, S.; Fassbender, D.; Vacca, A.; Busquets, E. A high-efficient solution for electro-hydraulic actuators with energy regeneration capability—ScienceDirect. *Energy* **2020**, *216*, 119291. [CrossRef]
28. Lin, T.; Wang, Q.; Hu, B.; Gong, W. Research on the energy regeneration systems for hybrid hydraulic excavators. *Autom. Constr.* **2010**, *19*, 1016–1026. [CrossRef]
29. Xu, J.; Yoon, H.S. A review on mechanical and hydraulic system modeling of excavator manipulator system. *J. Constr. Eng.* **2016**, *2016*, 9409370. [CrossRef]
30. Ronkkonen, J.; Kukkonen, S.; Price, K.V. Real-parameter optimization with differential evolution. In Proceedings of the 2005 IEEE Congress on Evolutionary Computation, Edinburgh, UK, 2–5 September 2005; Volume 1, pp. 506–513.
31. Suganthan, P.N.; Hansen, N.; Liang, J.J.; Deb, K.; Chen, Y.P.; Auger, A.; Tiwari, S. Problem Definitions and Evaluation Criteria for the CEC 2005 Special Session on Real-Parameter Optimization. *Nat. Comput.* **2005**, *2005*, 341–357.